Saponite-anthocyanin pigments: Slipping between the sheets

Luciano Clécio Brandão Lima, Fabrícia Castro-Silva, Edson Cavalcanti Silva-Filho, Maria Gardennia Fonseca, Maguy Jaber

To cite this version:

Luciano Clécio Brandão Lima, Fabrícia Castro-Silva, Edson Cavalcanti Silva-Filho, Maria Gardennia Fonseca, Maguy Jaber. Saponite-anthocyanin pigments: Slipping between the sheets. Microporous and Mesoporous Materials, 2020, 300, pp.110148. 10.1016/j.micromeso.2020.110148 . hal-02887318

HAL Id: hal-02887318
https://hal.sorbonne-universite.fr/hal-02887318v1

Submitted on 2 Jul 2020

Saponite-anthocyanin pigments: slipping between the sheets

Luciano Clécio Brandão Lima[1,2], Fabrícia Castro-Silva[1,2], Edson Cavalcanti Silva-Filho[1], Maria Gardênnia Fonseca[3], Maguy Jaber[2]*

[1]LIMAV, Univ. Federal do Piauí – UFPI, 64049-550 Piauí, Brazil
[2]Sorbonne Université, CNRS UMR 8220, LAMS, Institut Universitaire de France (IUF), case courrier 225, 4 pl. Jussieu 75252 Paris cedex 05, France
[3]NPE-LACOM, Univ. Federal da Paraíba – UFPB, João Pessoa, 58051-900 Paraíba, Brazil

ABSTRACT

The present work describes the synthesis and characterization of hybrid materials based on β-cyclodextrin (β-CD) and cetyltrimethylammonium bromide (CTAB) intercalated into saponite (SAP) and a commercially available powder of anthocyanin dye, Crystal Red Grape (RG). The interactions between the organic dye guest and the organo-clay host were investigated by X-ray diffraction, thermogravimetric analysis, transmission electronic microscopy and ^{13}C solid state nuclear magnetic resonance. The results support complex formation between β-CD and CTAB, their intercalation into the clay interlayer spaces or surface loading, and their interaction with RG (CTAB_SAP-RG, β-CD_SAP-RG and β-CD+CTAB_SAP-RG). The hybrid pigments formed exhibit different colors, enhanced stability against visible light irradiation and basic pH conditions. These hybrid pigments are environmentally friendly and can be promising candidates in different application fields.

KEYWORDS: Saponite, Natural dye, Adsorption, Hybrid pigment, Color change.

1. Introduction

The whole spectrum of colors obtained from natural sources has been employed and improved since the ancient civilization, but their use declined during the development of organic chemistry in 19th century, with the "boom" of synthetic dyes and pigments to get away from the limitations of natural dyes, which are subject to the growing seasons of the plants or the life-cycles of the insects [1,2].

This context has lead the researches into natural dyes to take main focus to historical, archaeological and cultural heritage aspects. However, in the last few decades, the efforts of producing dyes providing long-lasting coloring effect comes at the cost of complex organic structures and hazardous effects, reviving the age-old quest of humankind for natural resources, since the conventional uses of synthetic dyes have posed serious threat to global environment. In this way, the demand for eco-friendly products is switching the trend of using synthetic dyes over the use of naturally occurring colorants [3,4].

The anthocyanins are the natural pigments that humanity and animals have most consumed from the beginning of time. Anthocyanins are therefore a highly desirable substitute for synthetic food colors, being regarded to be non-toxic and strongly associated to the disease prevention activities found in their sources by opposition to the synthetic food pigments [5–7].

Anthocyanins are responsible for almost all nuances of blue, red, or purple pigments found in plants, especially flowers, fruits, and tubers. They are water-soluble glycosylated polyhydroxy and polymethoxy derivatives of 2-phenylbenzopyrylium (flavylium) salts that have a common C_6—C_3—C_6 structure consisting of two aromatic rings linked through an oxygenated heterocycle [8,9]. These molecules have an antioxidant and free-radical scavenging properties which promote their recognized anti-inflammatory, antitumor, anti-mutagenic, antiulcer, antiangiogenic, and antiaging activities in addition to its diabetes prevention.

Despite their use in several fields due to their mentioned properties, anthocyanins have limitations due to their photo- and chemical-stabilities [10]. Anthocyanin dyes are unstable at external environmental conditions such as light, pH, oxygen, temperature [11].

Therefore, biohybrid compounds that combine these biomolecules and an inorganic counterpart such as clay minerals have been widely investigated to reverse these limitations by complexation in the host materials [12–14]. This field of research has grown from studies about the first and most famous example of biohybrid, Maya blue, which is composed of a natural clay mineral (palygorskite) and indigo dye of biological origin [1,15,16].

The strategy to achieve the same stability known to Maya blue has been leading the scientists to try to enhance other organic dyes for several applications. Concerning the studies about anthocyanins, montmorillonite has been investigated as inorganic host materials in recent years [12,17,18], followed by palygorskite [19,20], sepiolite [21], laponite [22] and saponite [23]. However, no study explored the stability enhancement for anthocyanin after adsorption on modified clay.

Among the many different types of clay minerals, saponite is a 2:1 trioctahedral phyllosilicate belonging to smectite group, which shows interesting properties due to their intercalation/exfoliation characteristics, large specific surface area, surface acidity, cation exchange capacity, thermal stability, biocompatible, and non-toxic properties [24].

The structure of saponite is composed of a magnesium octahedral sheet sandwiched between two silicon tetrahedral sheets via sharing oxygen. Substitution of Si^{4+} cations by Al^{3+} cations in the tetrahedral layer confers a negative charge generally compensated by alkaline or alkaline earth cations located in the interlayer space. The general formula of saponite can be expressed as $M^{+}_{x}[Si_{4-X}Al_{X}][Mg_{3}]O_{10}(OH)_{2}\cdot nH_{2}O$, where M is the exchangeable interlayer cation, x ($0.2 \leq x \leq 1.2$) is the fraction of aluminum present in Si-O tetrahedral sheets, and n is the number of water molecules [25,26].

Due to its negatively charged surface, saponite can be modified through the replacement of the interlayer inorganic cations by organic ones. Structures with organic cations, for example with quaternary ammonium cations such as hexadecyltrimethylammonium bromide (CTAB), have been extensively studied to provide surfactant-modified clays which can acquire hydrophobic and organophilic characteristics via the interlayer exchange process. The characteristics of this composite make it a promising candidate for the incorporation of dyes and aromatic compounds [13,27–30].

Moreover, surface modification of clay minerals with biopolymers such as starch, cellulose, chitosan and cyclodextrin was also reported for several applications [31–34]. It can be noticed that the interaction between polysaccharides and anthocyanins has shown to be especially important to improve the stability of the latter [35,36]. Among the wide range of biopolymers, cyclodextrin has gained prominence due to its ability to form non-covalent inclusion complexes due to the adaptable hydrophobic tridimensional cavity. Cyclodextrin (CDs) are cyclic D-glucopyranose oligomers, which the most common are knows to have six, seven, or eight glucose units linked by 1,4-α-glucosidic bonds, termed as α-, β-, and γ-CDs, respectively [37,38].

In this work, we report on the synthesis and characterization of hybrid pigments based on saponite, as well as its equivalent modified with β-cyclodextrin (β-CD) and hexadecyltrimethylammonium bromide (CTAB), and a commercially available powdered of anthocyanin dye, Crystal Red Grape (RG). The interactions and structural characterizations were also carried out by different techniques to study the chemical- and photo-stabilities of the obtained pigments.

2. Materials and methods

2.1. Materials

Anthocyanin source was a Crystal Red Grape (RG) donated by San Joaquin Valley Concentrates (Fresno, CA, USA). Hexadecyltrimethylammonium bromide (CTAB), β-cyclodextrin (β-CD), citric acid, sodium citrate, sodium hydroxide, hydrochloric acid, and other applied chemicals were purchased from Aldrich or Sigma-Aldrich, all with an analytical grade and used without any previous purification.

2.2. Saponite synthesis

For the synthesis of sodium saponite, the reagents were mixed in the following order according to the following theoretical formula: $Na_{0.3}(Si_{3.7}Al_{0.3})Mg_3O_{10}(OH)_2$: deionized water, hydrofluoric acid (40%, wt), sodium acetate (99%, wt), magnesium acetate tetrehydrate (99%, wt), basic aluminum acetate (19%, wt) and silica (Aerosil 130). The resulted hydrogels were aged under stirring at room temperature for 2 h and then were autoclaved at 300 °C, 90 bars for 6 h. The autoclaves were cooled to room temperature and the products were washed thoroughly with distilled water and centrifuged. The solids were then dried at 50 °C for 24 h [26].

2.3. Synthesis of inclusion complex β-CD+CTAB.

The inclusion complex formed by reaction of β-CD with CTAB was prepared according to a method previously described (Yei et al., 2005) with modifications. Solutions of CTAB (5.59 mmol) and β-CD (16.8 mmol) in water (80 mL) were prepared and mixed at room temperature. The mixture was stirred at 70 °C for 8 h and then it was left to stand at room temperature overnight. The mixture became turbid and the complex was obtained as a white crystalline precipitate. The precipitated product was collected after centrifugation and dried at 70 °C. The complex was then washed several times with water to remove any uncomplexed β-CD and CTAB. Finally, the powder was dried at 60 °C for 24 h.

2.4. Synthesis of hybrids organo-clay composites

Following the method described in [39] with modifications, a suspension of saponite (SAP, 5 g) in distilled water (250 mL) was stirred overnight in a 500 mL flask. The organic molecules (β-CD, CTAB or β-CD+CTAB inclusion complex; 2 g) were dissolved in 10 mL of 1 N HCl solution and added dropwise at room temperature to the stirred aqueous solutions of SAP. After stirring the mixture for 3 h, the white precipitate was collected by centrifugation, washed with water until no bromide ion could be detected by an aqueous $AgNO_3$ solution, and then dried at 60 °C for 24 h. The O-SAP materials obtained are named β-CD_SAP, CTAB_SAP and β-CD+CTAB_SAP.

2.5. Adsorption studies

Anthocyanin powder (RG) was dissolved in 0.020 $mol\cdot L^{-1}$ citric acid buffer solution (sodium citrate, citric acid at pH 3.0) to prepare a 5000 $mg\cdot L^{-1}$ solution that was used as stock solution.

2.5.1 Effect of contact time on the adsorption

The kinetics adsorption of anthocyanin on the materials were carried out as follows: 20.0 mg of saponite (SAP) was added to 20.0 mL of 1000.0 $mg\cdot L^{-1}$ dye solution and reacted for a time range of 2-240 minutes under mechanical stirring at 150 rpm and 25 ºC at pH 3. The samples were then centrifuged and equilibrium dye concentrations were determined by UV-visible spectrophotometer (Model: Ocean optics, HR2000) at 525 nm.

The quantity (moles) of the dye fixed in the adsorbate (q_e) was determined by the Eq.(1),

$$q_e = \frac{(C_o - C_e) * V}{m} \qquad (1)$$

where C_0 and C_e are the initial and equilibrium concentrations in solution (mg·L^{-1}), m is the mass of the material in g and V is the volume of the solution used in mL.

Experimental results were adjusted to the pseudo-first [40], pseudo-second order [41] and Elovich [42] adsorption kinetic models as described the following Eqs. (2)–(4):

Pseudo-first order: $$\ln(q_{e,\exp} - q_t) = \ln q_{e,cal} - K_1 t \qquad (2)$$

Pseudo-second order: $$\frac{t}{q_t} = \frac{1}{K_2 q_{e,cal}{}^2} + \frac{1}{q_{e,cal}} t \qquad (3)$$

Elovich: $$q_t = \beta(\ln \alpha\beta) + \beta(\ln t) \qquad (4)$$

Where q_e and q_t mg·g^{-1} are the adsorption capacities at the equilibrium and in a time t (min) respectively. In the Eq. (4) α (mg·g^{-1} min^{-1}) and β (g·mg^{-1}) are the initial adsorption rates and Elovich constant related to the extent of surface coverage and also to the activation energy involved in chemisorption, respectively.

2.5.2 Effect of initial concentration on the adsorption

To investigate the influence of anthocyanin concentration on adsorption, 20 mg of saponite (SAP) was added to 20 mL of dye solution at the different initial dye concentration at the 100 to 5000 mg·L^{-1}. The mixture was stirred for 1 h at room temperature and then centrifuged to separate the adsorbent. The concentration of dye in supernatant was analyzed using UV-visible spectrophotometer as described in previous subsection.

Experimental results were adjusted to Langmuir [43], Freundlich [44] and Temkin [45] models following the Eqs. (5)–(7):

Langmuir: $$\frac{C_e}{q_e} = \frac{1}{K_L q_m} + \frac{C_e}{q_m} \quad (5)$$

Freundlich: $$\ln q_e = \frac{1}{n_F} \ln C_e + \ln K_F \quad (6)$$

Temkin: $$q_e = \frac{1}{n_T} \ln K_T + \frac{1}{n_T} \ln C_e \quad (7)$$

Where C_e (mg·L^{-1}) is the dye equilibrium concentration, q_e (mg·g^{-1}) is the dye adsorbed amount on solid/liquid interface, q_{max} (mg·g^{-1}) is the maximum removal to form a monolayer of the dye on surface, K_L (L·mg^{-1}) is the Langmuir constant.

In the Freundlich model K_F (mg·g^{-1}) (mg·L^{-1})$^{-1/n}$ and n_F are the Freundlich constant and a factor which are related to capacity and intensity of the adsorption, respectively. For Temkin model, n_T is the constant related to adsorption energy (J·mol^{-1}), K_T (L mg^{-1}) is the Temkin isotherm constant, R is the gas constant (8.314 J·mol^{-1}·K) and T is the temperature (K).

2.6 Synthesis of the hybrid pigments

1 g of SAP or each O-SAP were dispersed in 100 mL of anthocyanin (RG) citric acid buffer solution at pH 3 (the RG concentration was 100 mg·L^{-1}) and was left under stirring for 1 h. The samples were then centrifuged and dried at 50 °C for overnight. The hybrid pigments samples are named SAP-RG, β-CD_SAP-RG, CTAB_SAP-RG and β-CD+CTAB_SAP-RG.

2.7. Characterizations.

X-ray diffraction were recorded using D8 Advance Bruker-AXS Powder X-ray diffractometer with CuKα radiation (λ = 1.5405 Å). XRD patterns were performed between 4-70° (2θ) with scan rate of 0.5 deg·min^{-1}.

Infrared analyzes were performed on Agilent Cary 630 FTIR spectrometer using an Agilent diamond Attenuated Total Reflectance (ATR) technique mode, with a spectral resolution > 2 cm^{-1} and 32 scans. Spectra were acquired by Microlab FTIR Software (Agilent Technologies) between 4000 and 650 cm^{-1}.

Thermogravimetric analyses were carried out using a TA Instrument SDT Q600 analyzer. The heating rate was of 5 $°C \cdot min^{-1}$ from 25 °C to 1000 °C, under dry air flow of 10 $mL \cdot min^{-1}$, and using alumina pan.

TEM study of the samples was performed on a JEOL 2010 microscope, 200 kV LaB_6 coupled Orius camera, from Gatan Company. Samples in the form of bulk powders were suspended in ethanol and then deposited on 400 mesh copper grids covered with an ultrathin carbon membrane of 2–3 nm thickness.

MAS NMR spectra were obtained on a Bruker Avance III spectrometer equipped with a 4 mm H-X MAS probe, operating at frequency of 500.17 MHz (^1H), 125.77 MHz (^{13}C). Chemical shifts were calibrated using the carboxyl signal of adamantane (38.52 ppm) for ^{13}C.

The ^{13}C Cross-Polarization spectra were acquired with a MAS rate of 14 kHz, a ramp-CP contact time of 1 m s and a 1 s recycle delay and with a ^1H decoupling spinal. Over an acquisition time of 40 m s, the number of scans to obtain the spectra depends on the S/N obtained for each sample. Spectra were processed with a zero-filling factor of 2 and with an exponential decay corresponding to a 25 Hz line broadening in the transformed spectra. Only spectra with the same line broadening are directly compared.

2.8. Chemical and photo-stabilities of the hybrid pigments

Chemical stability of anthocyanin molecules loaded on the matrix was verified by exposure of the hybrid pigments to basic and acidic conditions in a desiccator containing aqueous NH_4OH or HCl. At first, the sample was exposed to NH_3 atmosphere. After exposure to basic environment, the samples were transferred into a desiccator filled with HCl atmosphere. The sample was exposed to NH_3 and HCl atmospheres, sequentially and repeatedly [23].

The photo-stabilities were evaluated by exposure of solid pigments to white light irradiation for 192 h, using a LED lamp set to provide 100 Klx of illumination intensity, in which this time is equivalent to approximately 30 years of exposure in ambient light conditions. To study the effects of irradiation under oxidant and inert atmospheres, the pressed pigments (into pellets) were placed in a desiccator filled with air or nitrogen.

The absorbance, reflectance and CIE (Commission Internationale de L'Eclairage) parameters were obtained from an Ocean Optics Halogen and Deuterium Light Source HL-2000-FHSA device as incident light beam and ocean optics USB4000 detector for acquisition. Ocean Optics QP400-1-UV-VIS fiberglass was used to link these devices. For each acquisition, the optimum signal was obtain with an average of 100 scans. The diffuse reflectance (R) converted into equivalent absorption coefficient F(R) using Kubelka–Munk equation (Eq. (1)) [46].

$$F(R) = \frac{(1-R)^2}{2R} \tag{1}$$

The "Commission Internationale of l'Eclairage" CIE 1976 color space system was applied to evaluate the color of the pigments. Measurements were done on pressed pellets samples as function of L*, a* and b* coordinates. The differences of colors between unexposed and exposed samples were calculated by $\sqrt{((\Delta L^*)^2 + (\Delta a^*)^2 + (\Delta b^*)^2)}$ equation.

3. Results and Discussion

3.1 X-Ray Diffraction

XRD patterns of the pure CTAB shows typical reflections at 6.83°, 10.23°, 13.63°, 16.90°, 20.55°, 21.47°, 23.83°, 37.95°, 40.18 (JCPDS 00-030-1746) (Fig. 1A.). Characteristic reflections of β-CD are observed in 4.53°, 9.04°, 12.70°, 13.58°, 14.75°, 17.94°, 18.86°, 21.28°, 22.83°, 24.38°, 25.78°, 27.18°, 32.04° and 34.92° in agreement with previous works [47,48]. The XRD pattern of the product resulting from the mixture of cyclodextrin host and CTAB (β-CD+CTAB inclusion complex) is not a simple mixture of the two precursors but a new crystalline phase [37]. The differences observed between the patterns of their precursors were: i) the absence of the sharp and intense reflections of β-CD and CTAB (i.e. 4.53°, 9.04° for β-CD and 16.90°, for CTAB), ii) other ones shifted (i.e. 14.75°, 18.86° for β-CD and 13.63°, 20.55°, 21.47° for CTAB) and iii) presence of medium intense reflections after complexation (i.e. 14.75°, 18.86° for β-CD and 13.63°, 20.55°, 21.47° for CTAB), due to the encapsulation of the surfactant into the nano-hydrophobic cavities of β-CD [38,39].

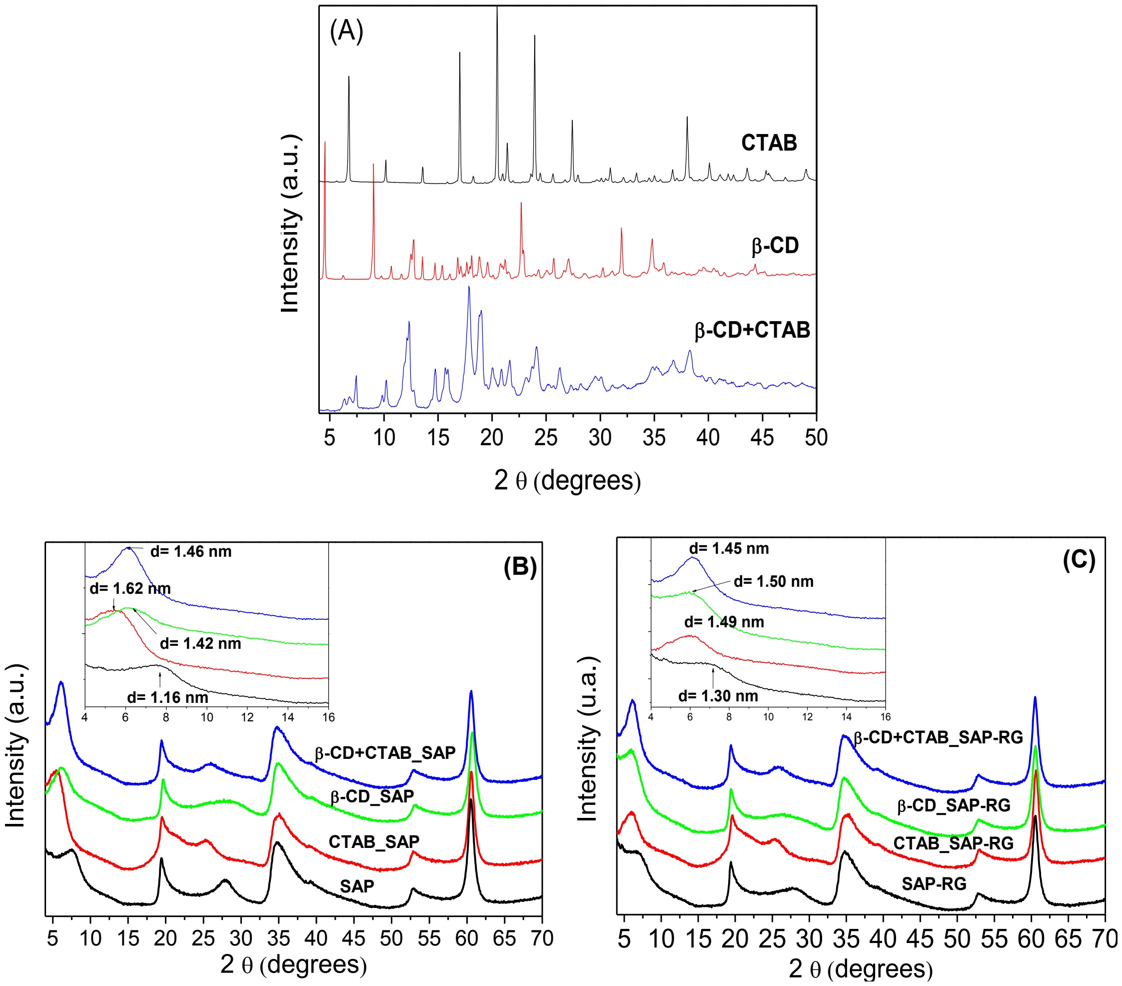

Fig. 1. X-ray diffractograms of (A) CTAB, β-CD and β-CD+CTAB; (B) SAP, CTAB_SAP, β-CD_SAP and β-CD+CTAB_SAP; (C) SAP-RG, CTAB_SAP-RG, β-CD_SAP-RG and β-CD+CTAB_SAP-RG.

The XRD patterns of the sodium saponite (Fig. 1B) showed typical (hkl) reflections of the clay and confirmed the success of the synthesis. The reflection at 7.66° (2θ) was associated to the basal spacing, $d_{(001)}$ of 1.16 nm, which can be correlated with a thickness of monohydrated sodium saponite layer [49].

After loading of the organic molecules in SAP, the initial basal spacing increased to 1.62 nm in CTAB_SAP, 1.42 nm in β-CD_SAP and 1.46 nm in β-CD+CTAB_SAP (Fig. 1B).

Different scenarios can be considered: for CTAB_SAP sample, the process involves cation exchange between CTA^+ and Na^+. The orientation of the organic chain in the interlayer space was suggested considering the dimensions of CTA^+ moieties

(Fig. 2) and the free interlayer space, which value was 0.65 nm for CTAB_SAP, corresponding to the difference between the SAP layer thickness and the basal spacing 1.62 nm. Therefore, the results are consistent with a monolayer arrangement of the organic molecules, where the ammonium groups tethered to the clay surface, and the alkyl chains lay parallel to the layers [50].

In the β-CD_SAP sample, since the d_{001} didn’t increase significantly considering the size of β-CD, one plausible hypothesis is the adsorption of the organic part on the surface of the layers and maybe on the edges via hydrogen bonding.

For β-CD+CTAB_SAP, a partial intercalation of the β-CD+CTAB complex can be proposed by ion exchange reaction between interlayer sodium cations of the SAP and positively charged portion of the inclusion complex.

For SAP and β-CD-SAP samples loaded with anthocyanin, the (001) reflexion was broader with a slightly increase of $d_{(001)}$ values, suggesting maybe a heterogeneity in the layer stacking due to dye intercalation. For CTAB_SAP after dye loading, the (001) reflexion was also broader but with a slight decrease of $d_{(001)}$ values. In this case, a partial release of of CTA^+ intercalated that convert the anthocyanin from the flavylium cation (AH_2^+) to quinoidal base form (AH) can occur, attenuating the electrostatic repulsions by forming the pair CTA+/AH on the SAP surface or into interlayer space. This can also explain the blue color of the pigment and the heterogeneity in the layer stacking. However, no change was observed in the d_{001} values of β-CD+CTAB-SAP samples after dye loading suggesting RG loading on the surfaces. Fig. 2 illustrates these all possibilities.

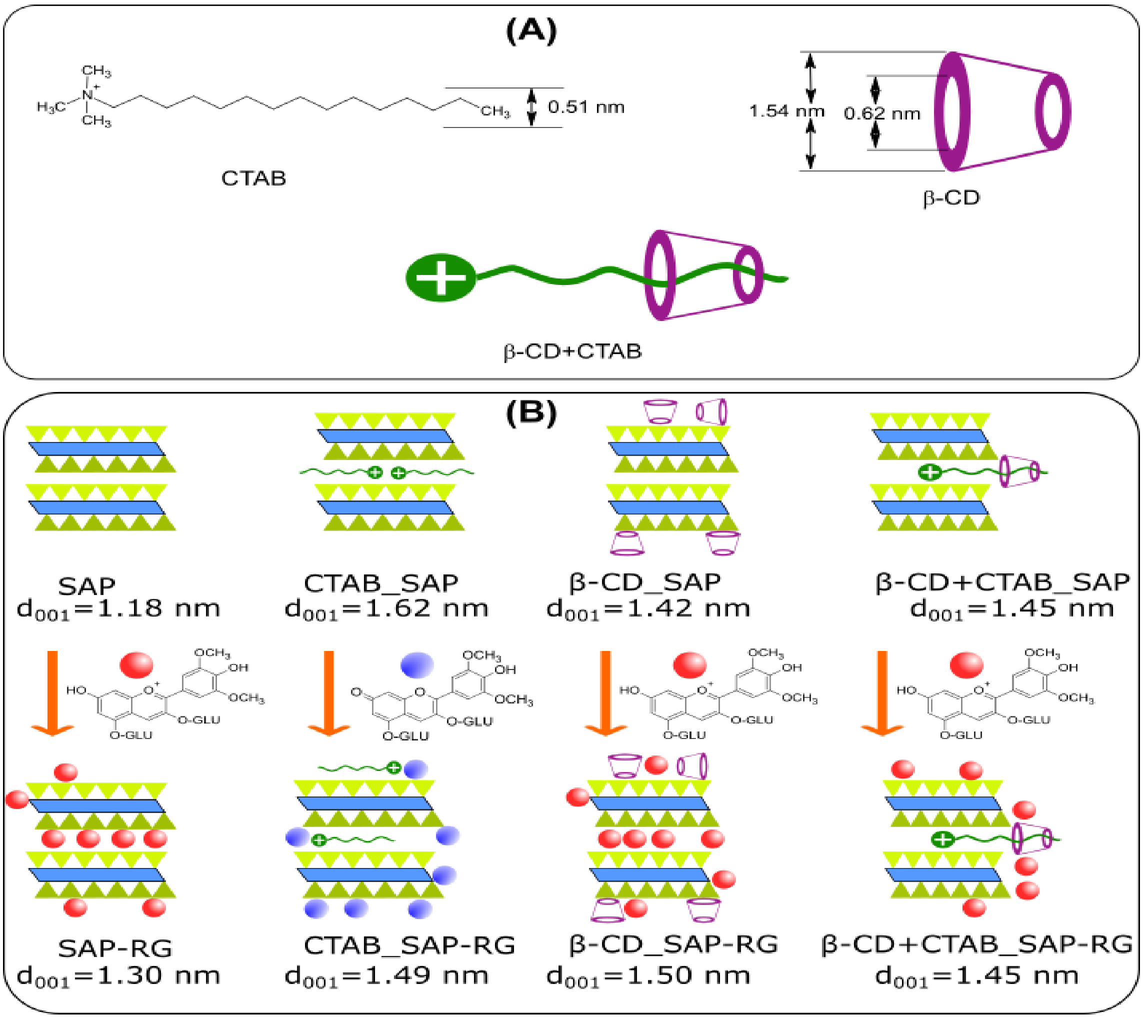

Fig. 2. Schematic representation of the (A) inclusion complex β-CD+CTAB and (B) hybrid formation.

3.2 Morphological analysis

TEM micrographs showed layers with alternate dark and bright fringes allowing the measurement of interplanar distances.

For pristine SAP, an interlayer distance of 1.19±0.11 nm was obtained (Fig. 3A). In O-SAP samples, the interlayer distance increased to 1.57±0.19 nm, 1.41±0.13 nm and 1.43±0.13 nm for CTAB_SAP, β-CD_SAP and β-CD+CTAB_SAP respectively (Fig. 3 C;E and G). After loading the anthocyanin molecules, the d_{001} spacing were 1.39±0.19, 1.49±0.20, 1.51±0.19 and 1.43±0.19 nm for SAP-RG, CTAB_SAP-RG, β-CD_SAP-RG and β-CD+CTAB_SAP-RG, respectively (Fig. 3 B;D;F and G). The values corroborated with the XRD data.

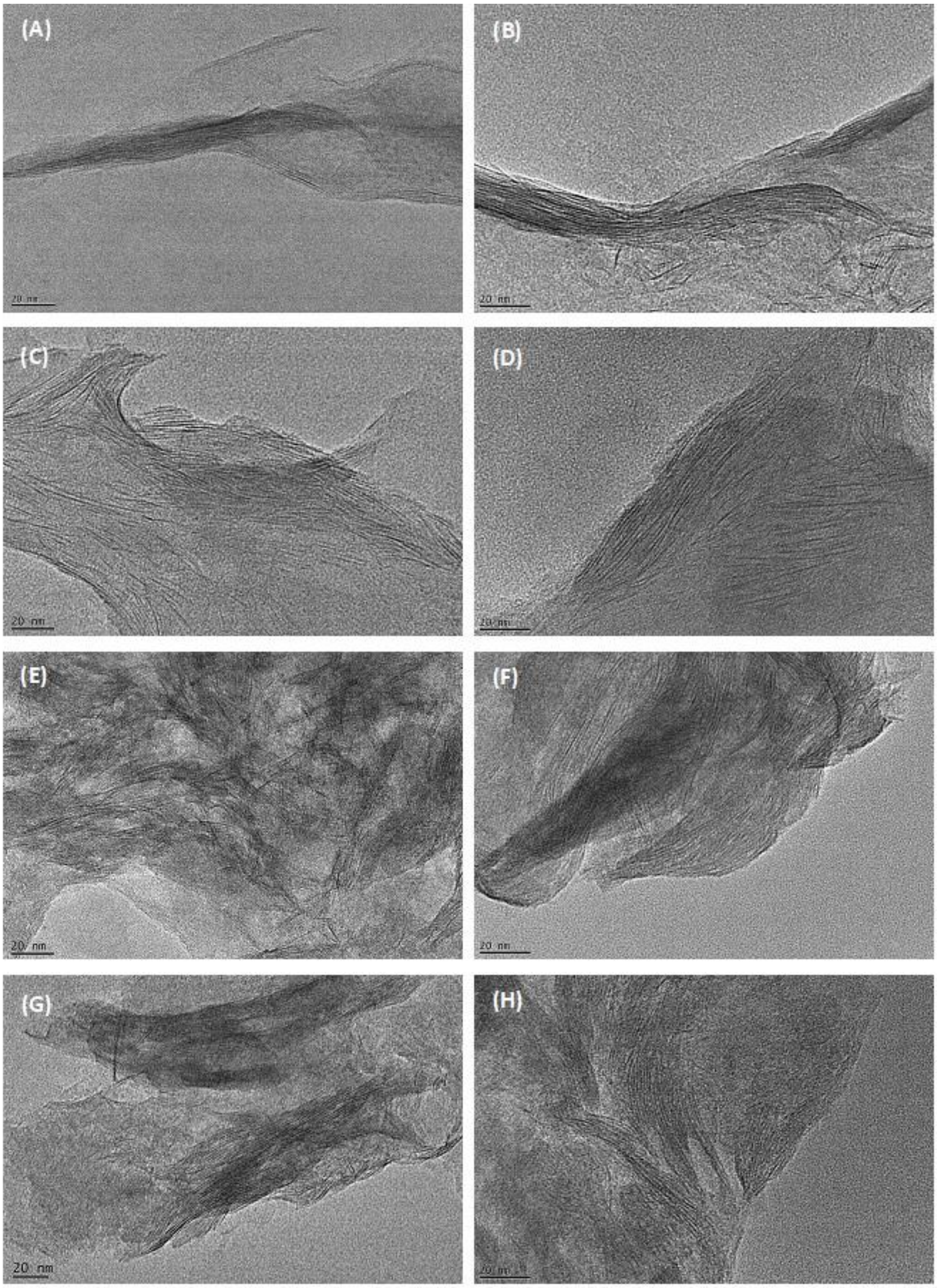

Fig. 3. TEM images of (A) SAP; (B) SAP-RG; (C) CTAB_SAP; (D) CTAB_SAP-RG; (E) β-CD_SAP; (F) β-CD_SAP-RG; (G) β-CD+CTAB_SAP and (H) β-CD+CTAB_SAP-RG.

3.3 FTIR

The infrared spectra of pure β-CD indicated its main absorptions at 3280 and 2925 cm^{-1} (Fig. 4A) attributed to ν(O−H) and ν(C−H), as well as the bands at 1152, 1077, 1023, and 940 cm^{-1} (Fig. 4B) assigned to δ(O−H), ν(C−C), and the α-1,4 linkage skeletal vibration, respectively [51,52].

The main bands associated to CTAB occurred at 3016, 2916 and 2847 cm^{-1} and were attributed to the $N(CH_3)_3$ asymmetric vibration, C-H and CH_2 asymmetric and symmetric stretching, respectively. Other bands in the range 1460-1488 cm^{-1} were assigned to $[N(CH_3)_3]$ and (CH_2) bending modes, while C-N vibrations were detected at 911 cm^{-1} and 963 [53,54].

The formation of the (β-CD)-(CTAB) complex attenuated the surfactant absorptions, due to the seven repeating units in the β-CD, the spectrum of the inclusion complex was largely dominated by the bands of the host portion, but even so, the spectra in Fig. 4A and Fig. 4B display some differences in comparison to spectra of their precursors that suggest the inclusion of CTAB into the β-CD cavity [51]. The band at 3280 cm^{-1} assigned to O-H stretching may correspond to the new hydrogen bonds in the complexes. The region between 2800-2980 cm^{-1} is attributed to ν(C−H) in β-CD+CTAB: it shows the contributions of the (CH) group in β-CD, shifted from 2925 cm^{-1} to 2919 cm^{-1}, and also a weak band at 2852 cm^{-1} related to the contribution of (CH_2) stretching of CTA^+, which appears as a shoulder probably due to the attenuation providing by the inclusion in the β-CD cavity. The bands at 1460-1488 cm^{-1} disappeared also suggesting the inclusion of the aliphatic chains in β-CD cavity, since these bands are mostly associated to the (CH_2) bending [55].

In Fig. 4C are shown the spectra of pristine SAP and the organoclays formed by intercalation of the surfactant, cyclodextrin and the inclusion complex represented by the CTAB_SAP, β-CD_SAP, β-CD+CTAB_SAP respectively.

For the SAP sample, the sharp and weak band at 3677 cm^{-1} and the region between 3000-3600 cm^{-1} are assigned to –OH vibrations modes. The band at 1633 cm^{-1} is attributed to –OH water bending. The band at 980 cm^{-1} was assigned to the Si-O-Si stretching [4,56].

After organomodification (Fig. 4C), the changes in CTAB_SAP spectra that confirm the presence of organic molecules are the new bands at 1478, 2847 and 2925, cm^{-1}, which were assign to the characteristic vibrations of CTAB alkyl chain. Concerning the β-CD_SAP spectrum, the different shape of the OH stretching and bending modes compared to the ones present in the pristine SAP suggests the contributions of OH groups brought from polysaccharide. A weak band at about 2924 cm^{-1} is attributed to ν(CH). Finally, the β-CD+CTAB_SAP sample shows more intense bands at 2853 and 2925 attributed to the CTAB alkyl chain in the β-CD+CTAB inclusion complex, in addition to the similar characteristics observed for β-CD_SAP.

The Fig. 4D presents the spectra of the natural dye (RG) and the hybrid pigments obtained. In the RG spectrum, the main bands related to the aromatic and phenolic structure of the anthocyanin can be seen in the following regions : 1250-1370 cm^{-1} and 1350-1530 cm^{-1} attributed to C-O and C-C modes, respectively [17,18], 1550-1700 cm^{-1} assigned to O-H bending and C=O stretching; and 3000-3700 cm^{-1} associated with stretching vibrations of O-H.

The presence of anthocyanin in the hybrids can be verified by the distinguished signal of –OH stretching and bending modes due to the contributions of anthocyanin bands and the appearance of the corresponding peaks in the region of 1320-1450 cm^{-}1, emerging in the FTIR spectrum of the hybrids.

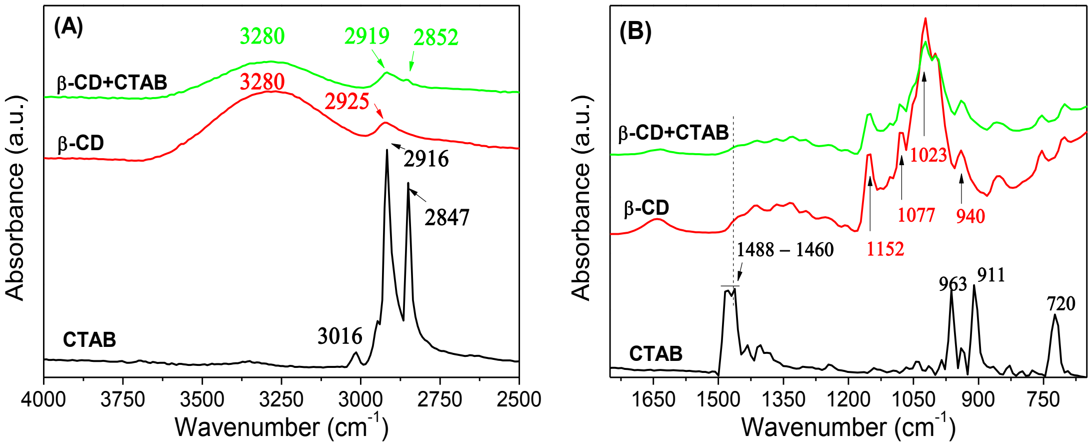

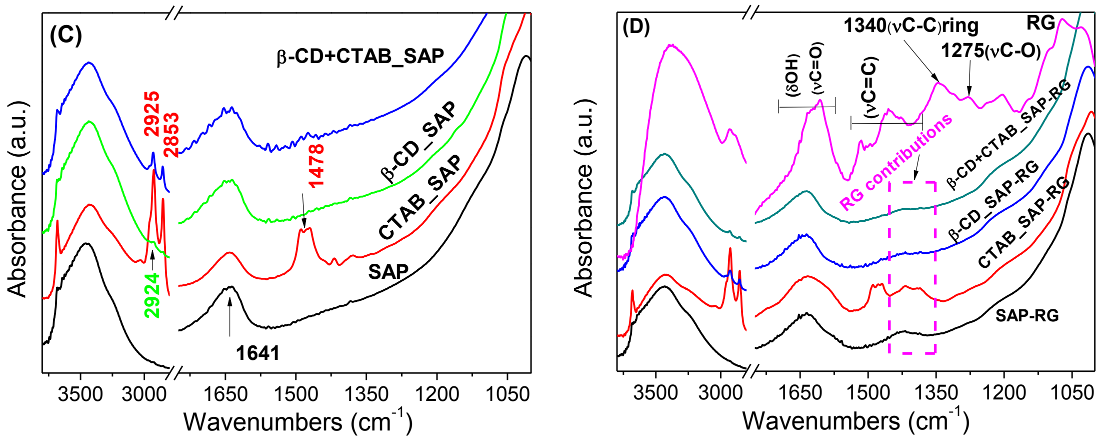

Fig. 4. FTIR spectra of (A-B) CTAB, β-CD and the inclusion complex β-CD+CTAB; (C) SAP and the organo-clay formed after incorporate CTAB, β-CD and β-CD+CTAB molecules; (D) hybrid pigments formed after adsorption of anthocyanin dye molecule in SAP, CTAB_SAP, β-CD_SAP and β-CD+CTAB_SAP.

3.4 ^{13}C MAS NMR

^{13}C MAS NMR spectra of β-CD+CTAB and their precursors are presented in Fig. 5A. The signals of CTAB occur in the chemical shift range of 10–70 ppm. The resonances at 16 ppm, 24 ppm and the complex signals that appear at 27-38 ppm are assigned to the terminal methyl group, the final methylene near to terminal methyl and the internal methylenes of the alkyl chain, respectively. The resonances at 55 ppm and 63 ppm are related to the $N\text{-}CH_3$ of the head-group and the first methylene group directly bonded to nitrogen, respectively [57]. The spectrum of β-CD shows the resonances of C1, C4 and C6 as multiple peaks that are spread over the chemical shift range of 100-107 ppm, 80-86 ppm and 57-65 ppm, respectively. It occurs due to asymmetric glucopyranosyl conformations. The chemical shift range of 68-77 ppm is related to the signals of C2, C5 and C3 [58].

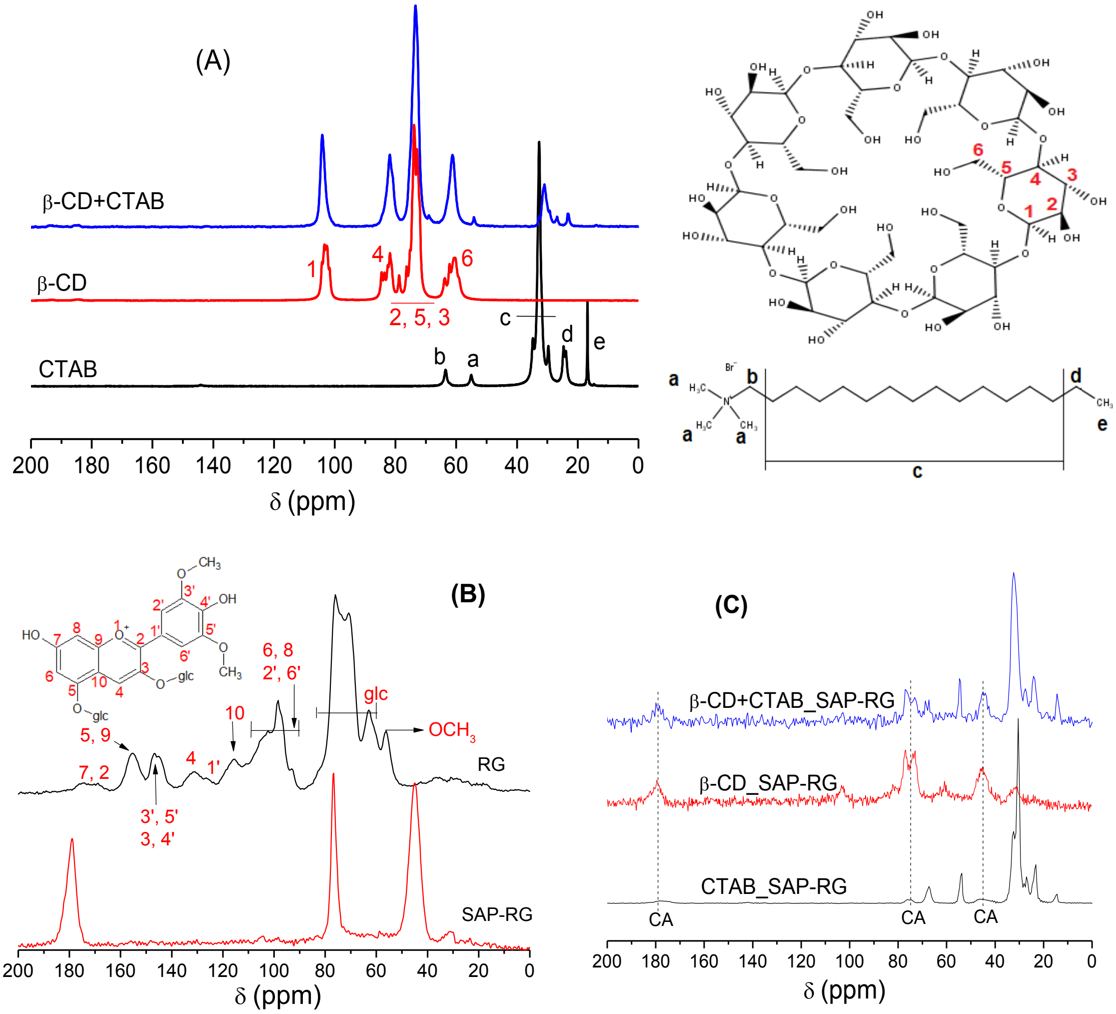

Fig. 5. ^{13}C MAS NMR spectra of (A) β-CD+CTAB and their precursors, (B) RG and SAP-RG, (C) CTAB_SAP-RG, β-CD_SAP-RG and β-CD+CTAB_SAP-RG.

The spectra of β-CD+CTAB complex (Fig. 5A) shows differences in comparison with the precursors. The resonances related to β-CD carbons appeared without significant shifts but as sharp singlet peaks after complexation, which implies that the β-CD unit adopts a symmetric cyclic conformation with the inclusion of CTAB alkyl chain. Changes in chemical shift confirm the interaction, as occurred in C(4) and C(6) glucopyranosyl monomer signals. For the CTAB signals, the peak assigned to terminal methyl group is absent, the peaks of methylene shifted from 24 ppm to 23 ppm and the complex signals related to internal methylenes shifted from the region of 27-38 ppm to 25-34 ppm. These changes indicate the inclusion of alkyl chain into β-CD hydrophobic cavity [39].

The ^{13}C MAS NMR spectra of the RG and the RG-SAP are presented in Fig. 5B, C. In the RG spectrum: the signal at 56 ppm is attributed to the OCH$_3$ groups bounded to the aglycone portion in C(3’) and C(5’) and the signals between 58-85 ppm are assigned to the chemical shifts of the glycosidic portions. The signals above 90 ppm are attributed to the aromatic carbons in flavylium cation, as indicated in Fig. 5B [59,60].

After incorporation of RG in SAP, any peaks in ^{13}C MAS NMR spectrum of the dye molecule was observed in the hybrid probably dominated by the other contributions. On the other hand, three signals at 45 ppm, 76 ppm and 179 ppm were assigned to the citric acid, which was also incorporated during the adsorption process. The same behavior is observed for CTAB_SAP-RG, β-CD_SAP-RG and β-CD+CTAB_SAP-RG (Fig. 5C) hybrids that showed peaks assigned to the organic precursors and also three signals of the citric acid (CA).

3.5 Thermal analyses

In Fig. 6A, the first step of degradation at 25-238 °C (mass loss about 8%) for raw SAP was assigned to the loss of physisorbed water and dehydration of interlayer cations. The second event at 640-859 °C is due to dehydroxylation of SAP with a weight loss of 3% [24,27]. DTG of SAP-RG shows an additionnal weight loss of 7% in the region 210-623 °C assigned to the degradation of the incorporated anthocyanin.

The weight losses in the second thermal event of O-SAP samples before the RG adsorption (Fig. 6B-D, Table 1) were 2%, 6% and 30% in β-CD_SAP, β-CD+CTAB_SAP and CTAB_SAP respectively. After dye loading, the organic mass losses increases to 6%, 8% and 32% for β-CD_SAP-RG, β-CD+CTAB_SAP-RG and CTAB_SAP-RG, respectively.

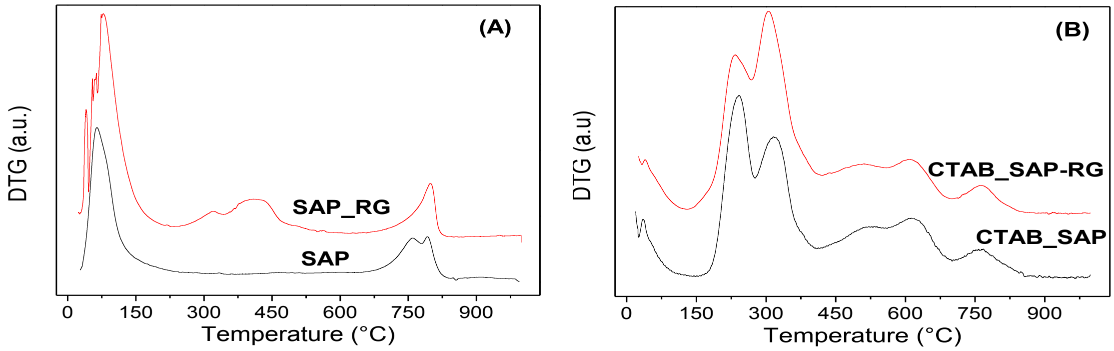

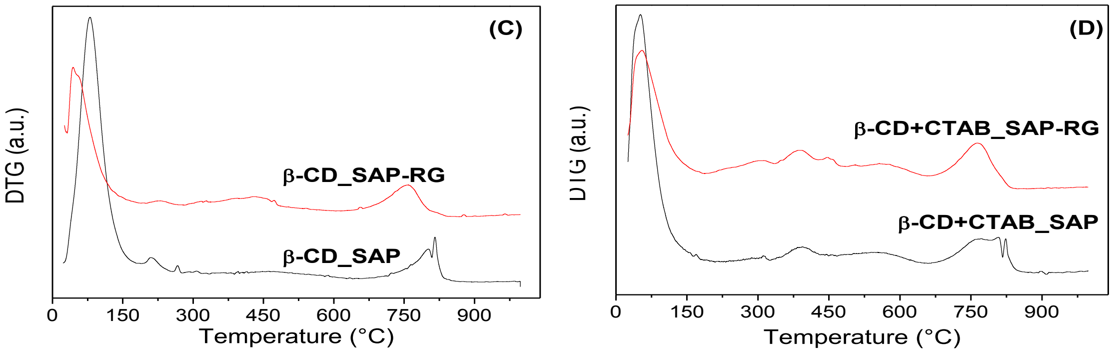

Fig. 6. DTG curve of (A) SAP and SAP-RG; (B) CTAB_SAP and CTAB_SAP-RG; (C) β-CD_SAP and β-CD_SAP-RG; (D) β-CD+CTAB_SAP and β-CD+CTAB_SAP-RG.

Table 1. Temperature range and percentages of mass loss observed in DTG curves.

Sample	**Temperature (^oC)**	**Mass loss (%)**
SAP	25-238	8.0
	640-859	3.5
SAP-RG	25-210	13.0
	210-623	7.2
	623-878	3.6
CTAB_SAP	25-117	2.4
	117-710	29.5
	710-878	2.9
CTAB_SAP-RG	25-125	2.4
	125-702	32.2
	702-888	2.5
β-CD_SAP	25-174	15.6
	174-319	2.5
	685-864	2.9
β-CD_SAP-RG	25-182	9.3
	182-600	5.9
	600-885	3.6
β-CD+CTAB_SAP	25-180	9.6
	180-670	6.1
	670-892	3.1
β-CD+CTAB_SAP-RG	25-181	6.5
	181-667	7.9
	667-885	3.0

3.6 Adsorption studies

3.6.1 Effect of the contact time

Adsorption kinetics studies were carried out and are depicted in Fig. 7.

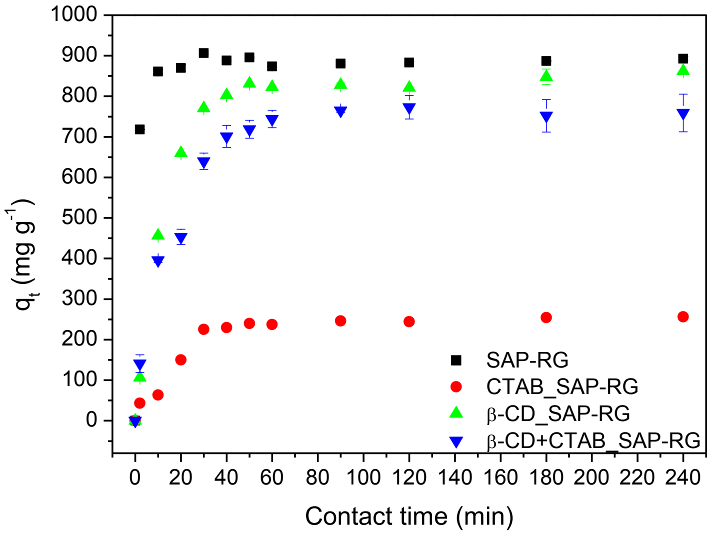

Fig. 7. Influence of the contact time on the RG adsorption on SAP; CTAB_SAP; β-CD_SAP; β-CD+CTAB_SAP samples.

The adsorption was fast during the first few minutes, mainly for raw saponite. The equilibrium times were reached after 10 min and resulted in dye adsorption capacity close to 910 mg·g^{-1} for SAP. For organo-saponite samples, the equilibrium times were achieved after 30, 50 and 60 min for CTAB_SAP, β-CD_SAP and β-CD+CTAB_SAP respectively, with lower maximum dye adsorption capacity than the pristine saponite. It is an indicative of the presence of different adsorption sites on organo-saponites.

In order to better understand the adsorption kinetics, the pseudo-first-order, pseudo-second-order and Elovich models were applied to experimental data and the resulted kinetic parameters of the fittings are presented in Table 2.

All systems were well-fitted to the pseudo-second order model, since that higher R^2 coefficient and low difference between the $q_{e,exp}$ and $q_{e,theor}$ were observed. Same results were obtained in other works [27,61].

Table 2. Kinetic parameters obtained by fitting the experimental data to pseudo-first order, pseudo-second order and Elovich models in the RG adsorption data by the organo-saponites.

Pseudo-first order				
Hybrid	$q_{e,exp}$ (mg·g^{-1})	$q_{e,cal}$ (mg·g^{-1})	k_1 10^{-2} (min^{-1})	R^2
SAP	906.71	45.30	0.57	0.2278
CTAB_SAP	256.02	118.21	2.43	0.8289
β-CD_SAP	862.09	234.27	1.83	0.6138
β-CD+CTAB_SAP	773.30	111.94	2.74	0.0411
Pseudo-second order				
Hybrid	$q_{e,exp}$ (mg·g^{-1})	$q_{e,cal}$ (mg·g^{-1})	K_2 10^{-2} (g·mg^{-1}·min^{-1})	R^2
SAP	906.71	892.86	243.89	0.9999
CTAB_SAP	256.02	273.22	7.59	0.9891
β-CD_SAP	862.09	892.86	13.49	0.9979
β-CD+CTAB_SAP	773.30	793.65	13.32	0.9976
Elovich				
Hybrid	$q_{e,exp}$ (mg·g^{-1})	α (mg·g^{-1}·min^{-1})	β 10^{-2} (g·mg^{-1})	R^2
SAP	906.71	6.02 10^{12}	3.43	0.5653
CTAB_SAP	256.02	58.58	1.94	0.8179
β-CD_SAP	862.09	360.84	0.64	0.8313
β-CD+CTAB_SAP	773.30	284.55	0.72	0.8732

3.6.2 Effect of the initial dye concentration

Equilibrium isotherms are presented in Fig. 8. The equilibrium curves showed first an increasing in the adsorption capacity at high RG concentrations. Then a plateau is observed corresponding to the saturation of the active sites [62–64].

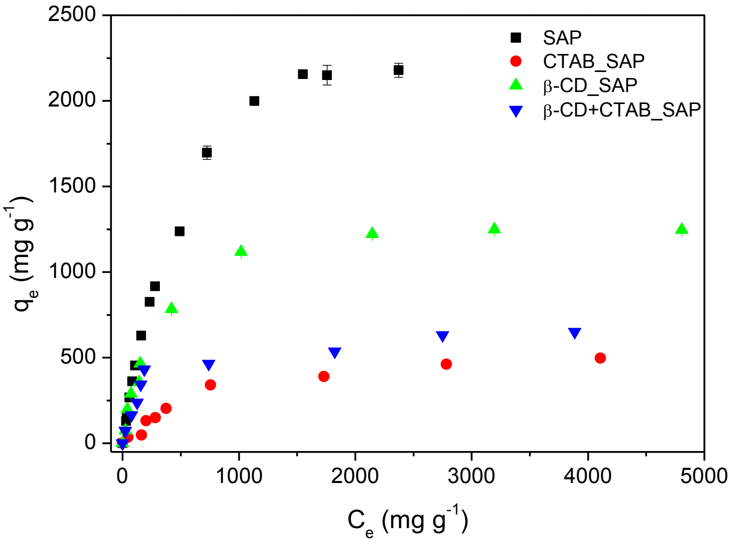

Fig. 8. Influence of the RG initial concentration on the adsorption process of SAP; CTAB_SAP; β-CD_SAP; β-CD+CTAB_SAP.

The saturation occurred at high RG initial concentration and resulted in high adsorption capacity for SAP-RG, (3500 mg·L^{-1} RG initial concentration and adsorption capacity about 2170.0 mg·g^{-1}). However for organo-saponite samples, equilibrium occurred at 3000.0, 1000.0 and 2500 mg·L^{-1} of RG initial concentrations and showed adsorption capacities close to 1230.0, 640 and 470 mg·g^{-1} for β-CD_SAP, β-CD+CTAB_SAP and CTAB_SAP respectively.

The equilibrium data were adjusted to Langmuir, Freundlich and Temkin models, and the resulting parameters are summarized in Table 3. The values of isotherm correlation coefficients revealed that the experimental data were well-fitted to Langmuir (R^2 closer to 1) compared with other models. Additionally, the R_L values calculated from the Langmuir equation suggested that the adsorption was favorable ($0 < R_L < 1$) in all cases. Adsorption sites in each sample were uniformly distributed on the surface and a monolayer adsorption took place [65].

Table 3. Parameters obtained by fitting the experimental data to Langmuir, Freundlich and Temkin models in the RG adsorption by the organo-saponites.

Langmuir				
Hybrid	$q_{e,exp}$ $(mg \cdot g^{-1})$	q_{max} $(mg \cdot g^{-1})$	R_L	R^2
SAP	2178.48	2819.06	0.21	0.9924
CTAB_SAP	462.24	595.24	0.66	0.9615
β-CD_SAP	1222.97	1343.35	0.19	0.9978
β-CD+CTAB_SAP	632.14	671.14	0.26	0.9967
Freundlich				
Hybrid	n_F $(mg \cdot g^{-1})$	K_F $(mg \cdot g^{-1})(mg \cdot L^{-1})^{-1/n}$		R^2
SAP	1.52	18.84		0.9596
CTAB_SAP	1.73	4.73		0.8716
β-CD_SAP	2.10	31.83		0.8797
β-CD+CTA_SAP	2.92	42.74		0.8025
Temkin				
Hybrid	n_T $(J \cdot mol^{-1})$	K_T 10^{-2} $(L \cdot mg^{-1})$		R^2
SAP	4.63	2.72		0.9646
CTAB_SAP	21.75	1.74		0.9512
β-CD_SAP	10.00	4.98		0.9675
β-CD+CTAB_SAP	23.20	10.63		0.9322

3.7 Chemical and photo-stabilities of the hybrid pigments

3.7.1 Spectra changes

The UV-Vis spectra of RG in citric acid solution buffered at pH 3 showed an absorption at 525 nm (Fig. 9A). The majority of anthocyanin molecules present in RG are malvidin-3,5-diglucoside, therefore the results are in concordance with the literature, that shows absorption around 520 nm for acid solution of anthocyanin [11,12,66].

The Fig. 9B shows the possible structural transformations of anthocyanin molecules in aqueous solution. The flavylium is the most stable form of anthocyanin that appears redish and turns to blue after conversion to quinoidal base when pH increases and finally to non- colored chalcone via hemicetal form.

Comparing the spectra of RG solution with those of hybrid pigments, a red shift occurred from 525 to 539 nm for SAP-RG, β-CD_SAP-RG, β-CD+CTAB_SAP-RG samples and 554 nm for CTAB_SAP-RG. The pH was adjusted by the addition of citric acid buffer solution during the hybrid pigment formation. Shifts in the absorptions can be related to electrostatic interactions between the clay mineral layer and the dye and/or by intramolecular interaction between the organic moieties in the respective hybrids.

The shift and presence of a broad band in the spectrum of CTAB_SAP-RG may indicate the deprotonation of the flavylium cations into deprotonate quinoidal base $AH_2 \rightleftharpoons AH$, which can be stabilized by electrostatic interaction with the positively charged surfactant in this hybrid system. This behavior may explain the blue color of the hybrid, while the other ones were weakly red.

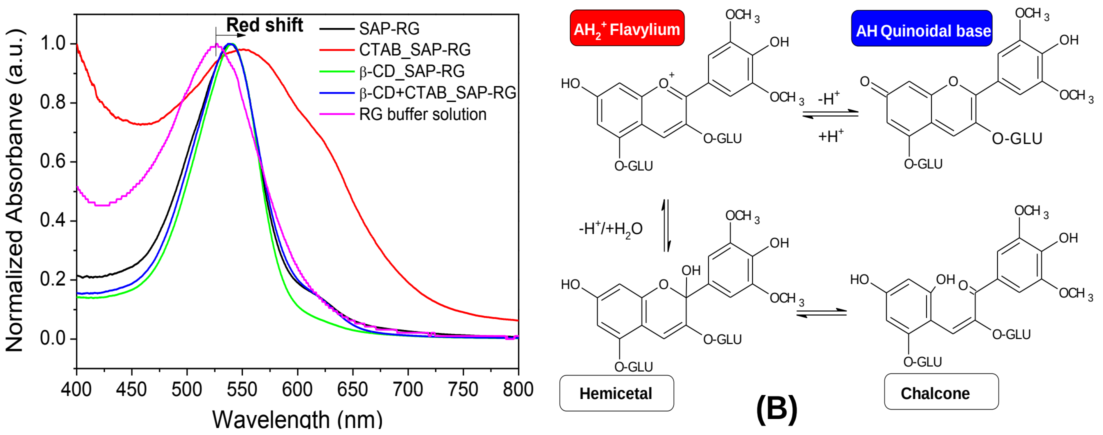

Fig. 9. (A) Diffuse reflectance UV–Vis spectra of hybrid pigments and the spectrum of RG citric acid buffer solution pH 3; (B) schematic representation of possible anthocyanin structures in different pHs in aqueous solution.

3.7.2 Color changes in acid/basic environments

The hybrid pigments were exposed to acidic or basic atmosphere prepared in a desiccator, in which the samples were submitted to HCl or NH_4OH atmosphere. The results upon exposure to acidic and basic vapors were monitored by visible absorption spectroscopy and also by visual changes in their photographs, these results are present in Fig. 10.

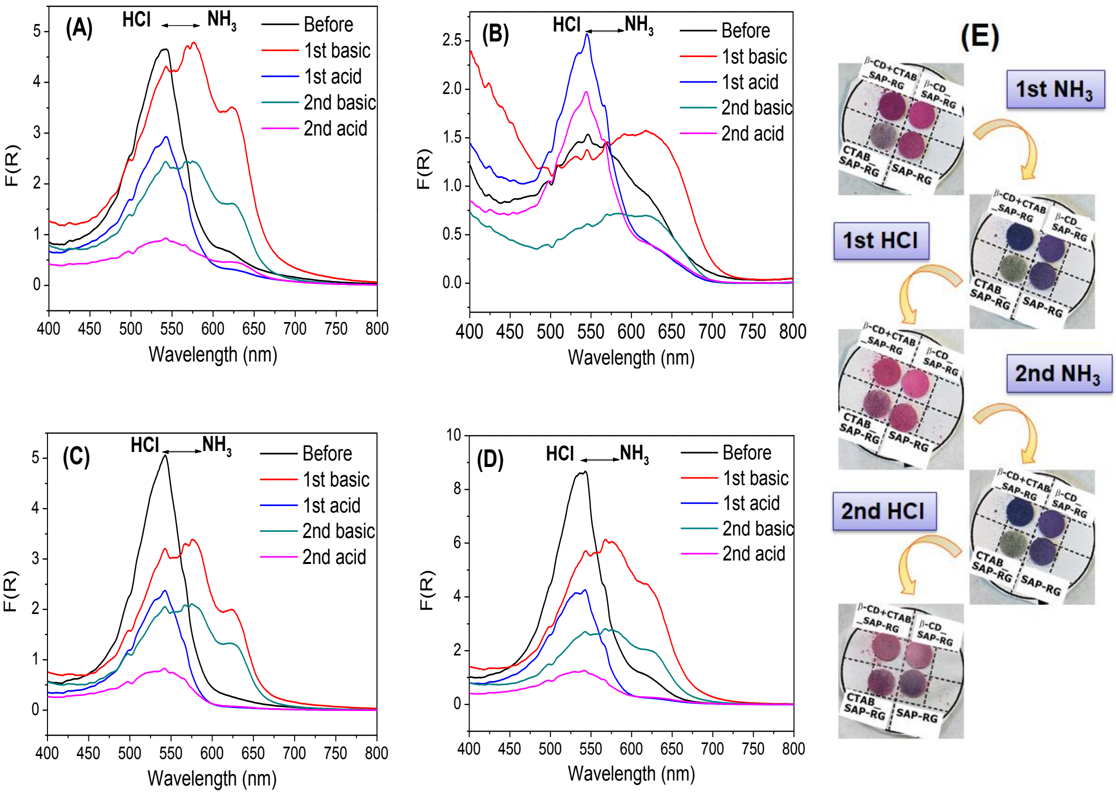

Fig. 10. Spectra changes after exposure to acidic and basic environments for (A) SAP-RG; (B) CTAB_SAP-RG; (C) β-CD_SAP-RG and (D) β-CD+CTAB_SAP-RG. (E) Digital photographs of the color changes of hybrid pigments upon exposure.

Colors changes from red to blue after exposure to basic atmosphere (NH_3 from aqueous NH_4OH) were observed in the SAP-RG, β-CD_SAP-RG and β-CD+CTAB_SAP-RG. The process is reversible, as shown in Fig. 10E. The exposure time to change the color was about 10 min. Similar results were obtained in the literature.

In Fig. 10(A, C and D), the absorption band have a redshift after exposure to basic atmosphere, and return to the same wavenumber, after exposure to basic atmosphere. After several cycles; the same observations on the spectra were noticed. The color change was reversible and repeatable for at least two cycles. The color changes are still observed after the second cycle of exposure, although strong acid and base conditions degraded the pigments.

The contribution of quinoidal base in the anthocyanin molecule in CTAB_SAP-RG was more pronounced than in the other hybrids and explains its initial blue color. After the first exposure to basic vapor, the right shift observed in Fig. 10B is due to the conversion of remaining flavylium cations to quinoidal base, which causes a change only in nuance of blue (Fig. 10E). Hybrids being exposed to basic conditions were again submitted to acidic environment, the color change to red and their spectra were similar to the other hybrids and indicated that the anthocyanin molecules became in flavylium cation form. The behavior of color change in the following cycles was also similar to the others hybrid pigments [18,20,23,32].

The decrease in relative absorbance is 80.4%, 73.8%, 83.2% and 84.3% for SAP-RG, CTAB_SAP-RG, β-CD_SAP-RG and β-CD+CTAB_SAP-RG respectively. These data indicate that the CTAB_SAP-RG has a slightly better chemical stability than the other pigments, since it has lowest decrease of relative absorbance after four cycles of acid basic exposure.

3.7.3 Photostability

The photostability of the hybrid pigments were studied under LED light exposure for 192 h under air and nitrogen atmosphere. Fig. 11 depicts the UV-Vis spectra.

The progressive decreasing in the absorbance at maximum wavelength occurred without differences in the spectral patterns, which indicated no simultaneous reaction that could form different derivatives chromophore species during the light exposure. Degradation were most pronounced in the process carried out under air for all hybrids. This behavior is expected since the photodegradation is often considered in relation to the oxidation caused by the evolution of singlet oxygen $^1O_2$ [12]. The order of fading of the hybrid pigments under air followed, CTAB_SAP-RG (75%) > β-CD+CTAB_SAP-RG (59%) > β-CD_SAP-RG (37%) > SAP-RG (34%).

On the other hand, the degree of degradation were about 18% (based on A/A0 = 0.82) for all hybrids under nitrogen atmosphere. The time exposure of the samples confirmed that the RG degradation process was less pronounced. Under nitrogen, reactive species are more difficult to form but the oxidation process remains possible due to the residual water molecules present in the pigments.

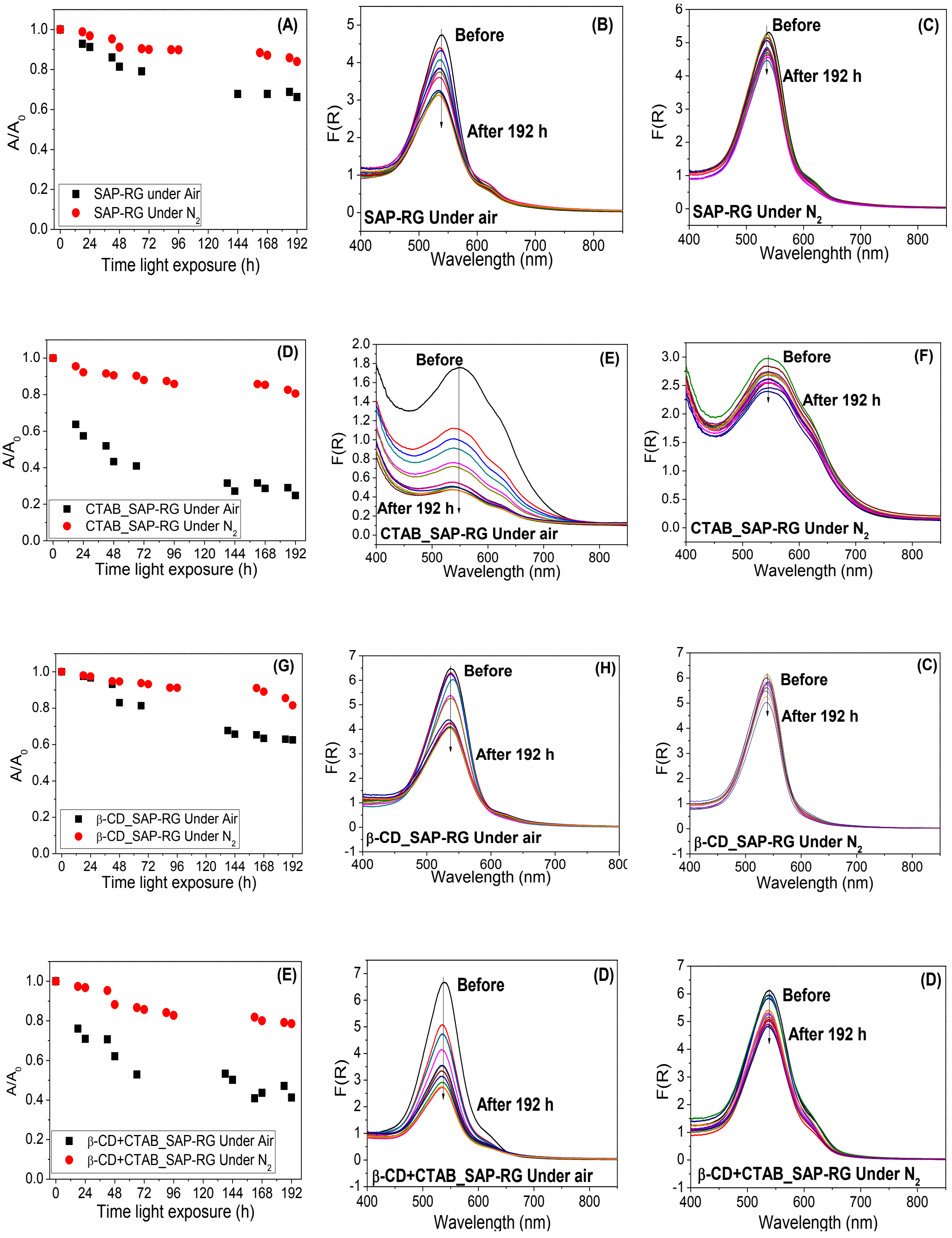

Fig. 11. Relative absorbance at λ_{max} and evolution of spectral patterns during light exposure for 192 h under air and nitrogen atmosphere for (A), (B) and (C) SAP-RG; (D), (E) and (F) CTAB_SAP-RG; (G), (H) and (I) β-CD_SAP-RG; (J), (K) and (L) β-CD+CTAB_SAP-RG.

The colors of solid hybrid pigments were evaluated before and after light exposure during 192 h (30 years of exposure in a museum). Measurements of L*a*b* parameters were carried out at different light irradiation times (Fig. 12).

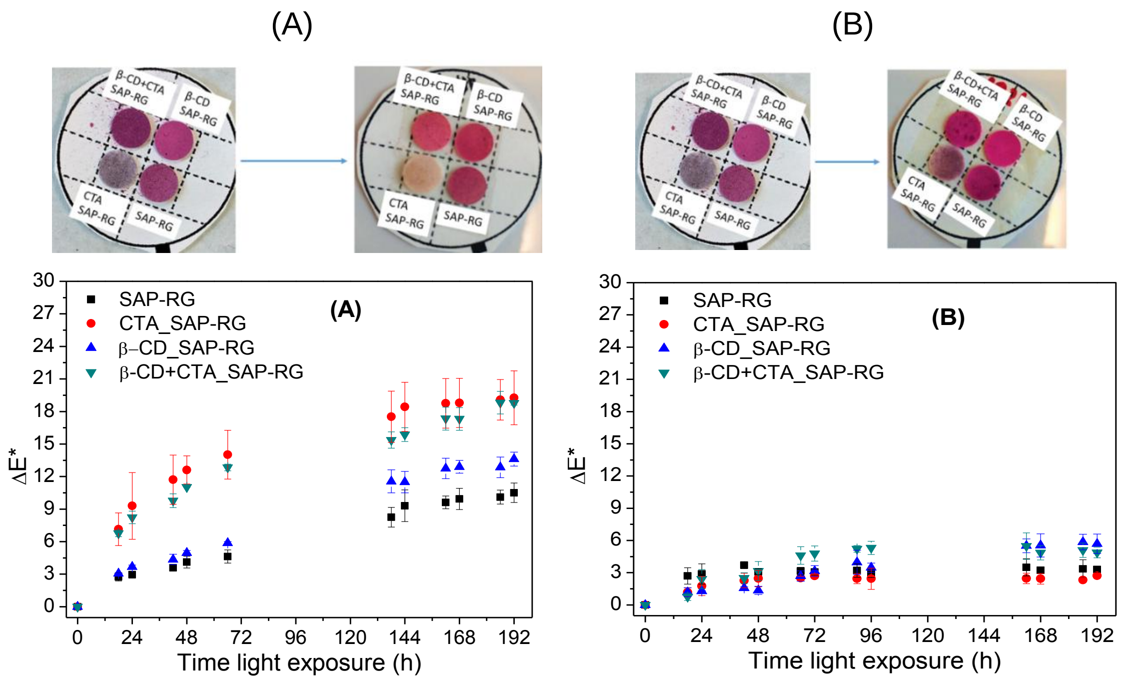

Fig. 12. Photo-ageing of pigments followed by color change observations over 192 h of light exposure under (A) air and (B) nitrogen atmosphere.

In solution, the color of RG changes from red in acid conditions to blue in neutral to weak alkaline conditions. However, the difference in color presented by the hybrids results from the different interactions between the host and the guest since the effect of pH on the color was controlled with the citric acid buffer solution. The color for SAP-RG is probably due to the intercalation of RG molecule in the interlayer space of SAP, which stabilizes the red color of flavylium cations. While adsorption in the CTAB_SAP-RG sample probably induced stabilization of the RG quinoidal base, leading to a blue color for the hybrid. The color for β-CD_SAP-RG is close to the one observed in SAP-RG and corroborates with the proposal of intercalation of the RG molecules in hybrids. Finally, the color for β-CD+CTAB_SAP-RG was between the colors of β-CD_SAP-RG and CTAB_SAP-RG, which is suggestive of a minor stabilization of RG quinoidal base than in CTAB_SAP-RG.

The ΔE* value is related to total color difference and is indicative of the light stability of the pigments. Under air (Fig. 12A), the ΔE* values of the pigments increased gradually with the increase of the ageing time. Finally, the values reached

10.5±0.9 for SAP-RG, 13.6±0.6 for β-CD_SAP-RG, 18.7±0.2 for β-CD+CTAB_SAP-RG and 19.3±2.5 for CTAB_SAP-RG after 192 h of light exposure. Lower ΔE* variation in SAP-RG and β-CD_SAP-RG under air is probably due to the protection of the dye in the interlayer space of the saponite creating an oxygen hindering and stabilizating the pigments under irradiation. Under nitrogen atmosphere, ΔE* values were lower after 192 h of light exposure, the ΔE* values were 2.7±0.2, 3.3±0.2, 4.8±0.5 and 5.7±0.9 for CTAB_SAP-RG, SAP-RG, β-CD+CTAB_SAP-RG and β-CD_SAP-RG, respectively. In addition, when the photostabilities under air are compared to photostabilities under nitrogen, the most significant differences were observed for β-CD+CTAB_SAP-RG and CTAB_SAP-RG, which corroborate with the greater exposure of RG molecules to oxygen attack on air atmosphere for these hybrids. The ΔE* values are summarized in Table 4.

Table 4. Total color differences (**ΔE***) for each sample after 192 h of light exposure under air and nitrogen atmosphere.

Sample	**ΔE* in air**	**ΔE* in N_2**
SAP-RG	10.5±0.9	3.3±0.2
CTAB_SAP-RG	19.3±2.5	2.7±0.2
β-CD_SAP-RG	13.6±0.6	5.7±0.9
β-CD+CTAB_SAP-RG	18.7±0.2	4.8±0.5

4 Conclusion

Hybrid pigments were successfully prepared by incorporating anthocyanin into unmodified and modified clay mineral based on synthetic SAP and CTAB and β-CD.

The hybrid pigments exhibit different colors function of their host-guest interactions. The presence of the quinoidal base form of anthocyanin molecule in CTAB_SAP-RG sample is probably more pronounced than in the other hybrids, which explains their initial blue color. The enhanced stability against visible light irradiation and basic environment conditions were brought by the electrostatic interaction between the dye and the respective host materials. The intercalation of the dye molecules into the interlayer spaces of saponite in β-CD_SAP-RG and SAP-RG protect the dyes from oxygen avoiding oxidation or the formation of other possible reactive oxygen species. Reversibility in color upon exposure to acidic and basic atmosphere is an evidence for a possible application of the obtained pigments as a sensor to atmospheric acidity, which can be exploited in several cycles if applied in less extreme pH conditions. These dyed materials are environmentally friendly and can be promising candidates in different application fields

Acknowledgments

We acknowledge the financial support from the CAPES/COFEBUB (Project n° 835/15), CAPES and National Council for Scientific and Technological Development (CNPq, Brazil) for financial support (Grant 310921/2017-1, M.G.F, 307460/2016-9, E.C.S.F.). The authors thank the Île-de-France region and CNRS for funding.

References

[1] G. Zhuang, F. Rodrigues, Z. Zhang, M.G. Fonseca, P. Walter, M. Jaber, Dressing protective clothing: stabilizing alizarin/halloysite hybrid pigment and beyond, Dye. Pigment. 166 (2019) 32–41. https://doi.org/10.1016/j.dyepig.2019.03.006.

[2] A.F. Vinha, F. Rodrigues, M.A. Nunes, M.B.P.P. Oliveira, Natural pigments and colorants in foods and beverages, Elsevier Inc., 2018. https://doi.org/10.1016/B978-0-12-813572-3.00011-7.

[3] K. Marszałek, Ł. Woźniak, B. Kruszewski, S. Skapska, The effect of high pressure techniques on the stability of anthocyanins in fruit and vegetables, Int. J. Mol. Sci. 18 (2017). https://doi.org/10.3390/ijms18020277.

[4] I. Fatimah, D. Rubiyanto, N.I. Prakoso, A. Yahya, Y.-L. Sim, Green conversion of citral and citronellal using tris(bipyridine)ruthenium(II)-supported saponite catalyst under microwave irradiation, Sustain. Chem. Pharm. 11 (2019) 61–70. https://doi.org/10.1016/J.SCP.2019.01.001.

[5] T.J. Lopes, M.G.N. Quadri, M.B. Quadri, Recovery of anthocyanins from red cabbage using sandy porous medium enriched with clay, Appl. Clay Sci. 37 (2007) 97–106. https://doi.org/10.1016/j.clay.2006.11.003.

[6] H.L. Ribeiro, E.S. Brito, M. de sá M. Souza Filho, H.M.C. Azeredo, Montmorillonite as a reinforcement and color stabilizer of gelatin films containing acerola juice, Appl. Clay Sci. 165 (2018) 1–7. https://doi.org/10.1016/j.clay.2018.07.041.

[7] E. Lima, P. Bosch, S. Loera, I.A. Ibarra, H. Laguna, V. Lara, Non-toxic hybrid pigments: Sequestering betanidin chromophores on inorganic matrices, Appl. Clay Sci. 42 (2009) 478–482. https://doi.org/10.1016/j.clay.2008.06.005.

[8] J.-L. Fang, Y. Luo, K. Yuan, Y. Guo, S.-H. Jin, Preparation and evaluation of an encapsulated anthocyanin complex for enhancing the stability of anthocyanin, LWT - Food Sci. Technol. 117 (2020) 1–8. https://doi.org/10.1016/J.LWT.2019.108543.

[9] R. Brouillard, Chemical Structure of Anthocyanins, in: P. Markakis (Ed.), Anthocyanins As Food Color., Academic Press, 1982: pp. 1–40. https://doi.org/10.1016/b978-0-12-472550-8.50005-6.

[10] B. Torres, B.K. Tiwari, A. Patras, P.J. Cullen, N. Brunton, C.P. O’Donnell, Stability of anthocyanins and ascorbic acid of high pressure processed blood orange juice during storage, Innov. Food Sci. Emerg. Technol. 12 (2011) 93–97. https://doi.org/10.1016/J.IFSET.2011.01.005.

[11] B. Piffaut, F. Kader, M. Girardin, M. Metche, Comparative degradation pathways of malvidin 3,5-diglucoside after enzymatic and thermal treatments, Food Chem. 50 (1994) 115–120. https://doi.org/10.1016/0308-8146(94)90106-6.

[12] Y. Kohno, R. Kinoshita, S. Ikoma, K. Yoda, M. Shibata, R. Matsushima, Y. Tomita, Y. Maeda, K. Kobayashi, Stabilization of natural anthocyanin by intercalation into montmorillonite, Appl. Clay Sci. 42 (2009) 519–523. https://doi.org/10.1016/j.clay.2008.06.012.

[13] P. Pimchan, N. Khaorapapong, M. Ogawa, The effect of cetyltrimethylammonium ion and type of smectites on the luminescence efficiency of bis(8-hydroxyquinoline)zinc(II) complex, Appl. Clay Sci. 101 (2014) 223–228. https://doi.org/10.1016/J.CLAY.2014.08.004.

[14] Â.A. Teixeira-Neto, C.M.S. Izumi, M.L.A. Temperini, A.M.D.C. Ferreira, V.R.L. Constantino, Hybrid materials based on smectite clays and nutraceutical anthocyanins from the Açaí fruit, Eur. J. Inorg. Chem. (2012) 5411–5420. https://doi.org/10.1002/ejic.201200702.

[15] G. Zhuang, M. Jaber, F. Rodrigues, B. Rigaud, P. Walter, Z. Zhang, A new durable pigment with hydrophobic surface based on natural nanotubes and indigo: Interactions and stability, J. Colloid Interface Sci. 552 (2019) 204–217. https://doi.org/10.1016/J.JCIS.2019.04.072.

[16] P. Trigueiro, F.A.R. Pereira, D. Guillermin, B. Rigaud, S. Balme, J.M. Janot,

I.M.G. dos Santos, M.G. Fonseca, P. Walter, M. Jaber, When anthraquinone dyes meet pillared montmorillonite: Stability or fading upon exposure to light?, Dye. Pigment. 159 (2018) 384–394. https://doi.org/10.1016/j.dyepig.2018.06.046.

[17] H.L. Ribeiro, A.V. de Oliveira, E.S. d. Brito, P.R.V. Ribeiro, M. de sá M. Souza Filho, H.M.C. Azeredo, Stabilizing effect of montmorillonite on acerola juice anthocyanins, Food Chem. 245 (2018) 966–973. https://doi.org/10.1016/j.foodchem.2017.11.076.

[18] S.M. Eskandarabadi, M. Mahmoudian, K.R. Farah, A. Abdali, E. Nozad, M. Enayati, Active intelligent packaging film based on ethylene vinyl acetate nanocomposite containing extracted anthocyanin, rosemary extract and ZnO/Fe-MMT nanoparticles, Food Packag. Shelf Life. 22 (2019) 100389. https://doi.org/10.1016/j.fpsl.2019.100389.

[19] S. Li, J. Ding, B. Mu, X. Wang, Y. Kang, A. Wang, Acid/base reversible allochroic anthocyanin/palygorskite hybrid pigments: Preparation, stability and potential applications, Dye. Pigment. 171 (2019) 107738. https://doi.org/10.1016/J.DYEPIG.2019.107738.

[20] G.T.M. Silva, C.P. Silva, M.H. Gehlen, J. Oake, C. Bohne, F.H. Quina, Organic/inorganic hybrid pigments from flavylium cations and palygorskite, Appl. Clay Sci. 162 (2018) 478–486. https://doi.org/10.1016/j.clay.2018.07.002.

[21] G.T.M. Silva, K.M. Da Silva, C.P. Silva, A.C.B. Rodrigues, J. Oake, M.H. Gehlen, C. Bohne, F.H. Quina, Highly fluorescent hybrid pigments from anthocyanin- and red wine pyranoanthocyanin-analogs adsorbed on sepiolite clay, Photochem. Photobiol. Sci. 18 (2019) 1750–1760. https://doi.org/10.1039/c9pp00141g.

[22] C. Capello, G.C. Leandro, C.E. Maduro Campos, D. Hotza, B.A. Mattar Carciofi, G.A. Valencia, Adsorption and desorption of eggplant peel anthocyanins on a synthetic layered silicate, J. Food Eng. 262 (2019) 162–169. https://doi.org/10.1016/J.JFOODENG.2019.06.010.

[23] M. Ogawa, R. Takee, Y. Okabe, Y. Seki, Bio-geo hybrid pigment; clay-anthocyanin complex which changes color depending on the atmosphere, Dye. Pigment. 139 (2017) 561–565. https://doi.org/10.1016/J.DYEPIG.2016.12.054.

[24] C. Zhang, H. He, Q. Tao, S. Ji, S. Li, L. Ma, X. Su, J. Zhu, Metal occupancy and its influence on thermal stability of synthetic saponites, Appl. Clay Sci. 135 (2017) 282–288. https://doi.org/10.1016/J.CLAY.2016.10.006.

[25] C.H. Zhou, Q. Zhou, Q.Q. Wu, S. Petit, X.C. Jiang, S.T. Xia, C.S. Li, W.H. Yu, Modification, hybridization and applications of saponite: An overview, Appl. Clay Sci. 168 (2019) 136–154. https://doi.org/10.1016/J.CLAY.2018.11.002.

[26] M. Jaber, J. Miéhé-Brendlé, Influence du milieu de synthése sur la cristallisation de saponite: Proposition de mécanisme réactionnel en milieux acide et basique, Comptes Rendus Chim. 8 (2005) 229–234. https://doi.org/10.1016/j.crci.2004.10.025.

[27] V. Tangaraj, J.-M. Janot, M. Jaber, M. Bechelany, S. Balme, Adsorption and photophysical properties of fluorescent dyes over montmorillonite and saponite modified by surfactant, Chemosphere. 184 (2017) 1355–1361. https://doi.org/10.1016/J.CHEMOSPHERE.2017.06.126.

[28] M. Polverejan, Y. Liu an, T. J.Pinnavaia, Mesostructured clay catalysts: a new porous clay heterostructure (PCH) derived from synthetic saponite, Stud. Surf. Sci. Catal. 129 (2000) 401–408. https://doi.org/10.1016/S0167-2991(00)80239-6.

[29] H. Han, M.K. Rafiq, T. Zhou, R. Xu, O. Mašek, X. Li, A critical review of clay-based composites with enhanced adsorption performance for metal and organic pollutants, J. Hazard. Mater. 369 (2019) 780–796. https://doi.org/10.1016/J.JHAZMAT.2019.02.003.

[30] F. Bergaya, M. Jaber, J. Lambert, Organophilic clay minerals, in: M. Galimberti (Ed.), Rubber Clay Nanocomposites. Sci. Technol. Appl., First Edit, J. Wiley & sons, 2011: pp. 45–86. https://doi.org/10.1002/9781118092866.ch2.

[31] V. Lozano-Morales, I. Gardi, S. Nir, T. Undabeytia, Removal of pharmaceuticals from water by clay-cationic starch sorbents, J. Clean. Prod. 190 (2018) 703–711. https://doi.org/10.1016/J.JCLEPRO.2018.04.174.

[32] M. Koosha, S. Hamedi, Intelligent Chitosan/PVA nanocomposite films containing black carrot anthocyanin and bentonite nanoclays with improved mechanical, thermal and antibacterial properties, Prog. Org. Coatings. 127 (2019) 338–347. https://doi.org/10.1016/J.PORGCOAT.2018.11.028.

[33] E. Abu-Danso, S. Peräniemi, T. Leiviskä, T. Kim, K.M. Tripathi, A. Bhatnagar, Synthesis of clay-cellulose biocomposite for the removal of toxic metal ions from aqueous medium, J. Hazard. Mater. 381 (2020) 120871. https://doi.org/10.1016/J.JHAZMAT.2019.120871.

[34] P. Mura, F. Maestrelli, C. Aguzzi, C. Viseras, Hybrid systems based on “drug – in cyclodextrin – in nanoclays” for improving oxaprozin dissolution properties,

Int. J. Pharm. 509 (2016) 8–15. https://doi.org/10.1016/J.IJPHARM.2016.05.028.

[35] I. Mourtzinos, D.P. Makris, K. Yannakopoulou, N. Kalogeropoulos, I. Michali, V.T. Karathanos, Thermal stability of anthocyanin extract of Hibiscus sabdariffa L. in the presence of β-cyclodextrin, J. Agric. Food Chem. 56 (2008) 10303–10310. https://doi.org/10.1021/jf801389j.

[36] M. Buchweitz, M. Speth, D.R. Kammerer, R. Carle, Impact of pectin type on the storage stability of black currant (Ribes nigrum L.) anthocyanins in pectic model solutions, Food Chem. 139 (2013) 1168–1178. https://doi.org/10.1016/J.FOODCHEM.2013.02.005.

[37] C.C. Rusa, C. Luca, A.E. Tonelli, Polymer-cyclodextrin inclusion compounds: Toward new aspects of their inclusion mechanism, Macromolecules. 34 (2001) 1318–1322. https://doi.org/10.1021/ma001868c.

[38] A. Bagheri, A.A. Rafati, Thermodynamic investigation of inclusion complex formation between cetyltrimethyl ammonium bromide (CTAB) and β-cyclodextrin at various temperatures, J. Mol. Liq. 195 (2014) 145–149. https://doi.org/10.1016/J.MOLLIQ.2014.02.020.

[39] D.-R. Yei, S.-W. Kuo, H.-K. Fu, F.-C. Chang, Enhanced thermal properties of PS nanocomposites formed from montmorillonite treated with a surfactant/cyclodextrin inclusion complex, Polymer (Guildf). 46 (2005) 741–750. https://doi.org/10.1016/J.POLYMER.2004.11.108.

[40] S. Lagergren, Zurtheorie der sogenannten adsorption gelosterstoffe, K. Vet. Akad. Handl. 24 (1898) 1–39.

[41] Y.. Ho, G. McKay, Pseudo-second order model for sorption processes, Process Biochem. 34 (1999) 451–465. https://doi.org/10.1016/S0032-9592(98)00112-5.

[42] S.Y. Elovich, L. G., Theory of adsorption from solutions of non electrolytes on solid (I) equation adsorption from solutions and the analysis of its simplest form, (ii) verification of the equation of adsorption isotherm from solutions, Izv. Sib. Otd. An. Khim. 2 (1962) 209–216.

[43] I. Langmuir, The adsorption of gases on plane surfaces of glass, mica and platinum, J. Am. Chem. Soc. 40 (1918) 1361–1403. https://doi.org/10.1021/ja02242a004.

[44] H. Freundlich, Über die Adsorption in Lösungen, Zeitschrift Für Phys. Chemie. 57U (1907). https://doi.org/10.1515/zpch-1907-5723.

[45] M.J. Temkin, V. Pyzhev, Recent modifications to Langmuir isotherms, Acta

Phys. Chim. 12 (1940) 217–222.

[46] G.T.M. Silva, C.P. Silva, M.H. Gehlen, J. Oake, C. Bohne, F.H. Quina, Organic/inorganic hybrid pigments from flavylium cations and palygorskite, Appl. Clay Sci. 162 (2018) 478–486. https://doi.org/10.1016/j.clay.2018.07.002.

[47] M. Kundu, S. Saha, M.N. Roy, Evidences for complexations of β-cyclodextrin with some amino acids by 1H NMR, surface tension, volumetric investigations and XRD, J. Mol. Liq. 240 (2017) 570–577. https://doi.org/10.1016/J.MOLLIQ.2017.05.123.

[48] S. Gao, Y. Liu, J. Jiang, Q. Ji, Y. Fu, L. Zhao, C. Li, F. Ye, Physicochemical properties and fungicidal activity of inclusion complexes of fungicide chlorothalonil with β-cyclodextrin and hydroxypropyl-β-cyclodextrin, J. Mol. Liq. 293 (2019) 111513. https://doi.org/10.1016/J.MOLLIQ.2019.111513.

[49] K. El Adraa, V. Timon, J.F. Lambert, A.R. Al-Rabaa, F. Jaber, M. Jaber, F. Tielens, Adsorption of l-DOPA intercalated in hydrated Na-saponite clay: A combined experimental and theoretical study, J. Phys. Chem. C. 116 (2012) 26414–26421. https://doi.org/10.1021/jp3094148.

[50] L. Marçal, E.H. De Faria, E.J. Nassar, R. Trujillano, N. Martín, M.A. Vicente, V. Rives, A. Gil, S.A. Korili, K.J. Ciuffi, Organically Modified Saponites: SAXS Study of Swelling and Application in Caffeine Removal, ACS Appl. Mater. Interfaces. 7 (2015) 10853–10862. https://doi.org/10.1021/acsami.5b01894.

[51] N. Li, L. Xu, Thermal analysis of β-cyclodextrin/Berberine chloride inclusion compounds, Thermochim. Acta. 499 (2010) 166–170. https://doi.org/10.1016/j.tca.2009.10.014.

[52] A.M. dos Santos Moreira, V.C.E. Bittencourt, F.L.S. Costa, M. Elena de Lima, M.T.P. Lopes, W.S. Borges, G.F. Martins, C.S. Nascimento, J.G. da Silva, Â.M.L. Denadai, K.B. Borges, Hydrophobic Nanoprecipitates of β-Cyclodextrin/Avermectins Inclusion Compounds Reveal Insecticide Activity against Aedes aegypti Larvae and Low Toxicity against Fibroblasts, J. Agric. Food Chem. 66 (2018) 7275–7285. https://doi.org/10.1021/acs.jafc.8b01300.

[53] A.F. Cortez Campos, P.H. Michels-Brito, F.G. da Silva, R.C. Gomes, G. Gomide, J. Depeyrot, Removal of direct yellow 12 from water using CTAB-coated core-shell bimagnetic nanoadsorbents, J. Environ. Chem. Eng. (2019) 103031. https://doi.org/10.1016/J.JECE.2019.103031.

[54] M. Mobarak, A.Q. Selim, E.A. Mohamed, M.K. Seliem, A superior adsorbent of

CTAB/H2O2 solution−modified organic carbon rich-clay for hexavalent chromium and methyl orange uptake from solutions, J. Mol. Liq. 259 (2018) 384–397. https://doi.org/10.1016/J.MOLLIQ.2018.02.014.

[55] T.M. De Miranda, A.R. De Oliveira, J.R. Pereira, J.G. Da Silva, I.S. Lula, C.S. Nascimento, Â.M. l. Denadai, Inclusion vs. micellization in the cethylpyridine chloride / β-cyclodextrin system: A structural and thermodynamic approach, J. Mol. Struct. 1184 (2019) 289–297. https://doi.org/S0022286019301632.

[56] Q. Tao, Y. Fang, T. Li, D. Zhang, M. Chen, S. Ji, H. He, S. Komarneni, H. Zhang, Y. Dong, Y.D. Noh, Silylation of saponite with 3-aminopropyltriethoxysilane, Appl. Clay Sci. 132–133 (2016) 133–139. https://doi.org/10.1016/J.CLAY.2016.05.026.

[57] J. Madejová, Ľ. Jankovič, M. Slaný, V. Hronský, Conformation heterogeneity of alkylammonium surfactants self-assembled on montmorillonite: Effect of head-group structure and temperature, Appl. Surf. Sci. 503 (2020) 144125. https://doi.org/10.1016/j.apsusc.2019.144125.

[58] S.J. Heyes, N.J. Clayden, M. Dobson, 13C-CP / MAS NMR studies of the cyclomalto-oligosaccharide (cyclodextrin) hydrates, 233 (1992) 1–14.

[59] N. Saito, K. Toki, T. Honda, K. Kawase, Cyanidin 3-malonylglucuronylglucoside in Bellis and cyanidin 3-malonylglucoside in Dendranthema, Phytochemistry. 27 (1988) 2963–2966. https://doi.org/10.1016/0031-9422(88)80697-6.

[60] M. Wolniak, I. Wawer, 13C CPMAS NMR and DFT calculations of anthocyanidins, Solid State Nucl. Magn. Reson. 34 (2008) 44–51. https://doi.org/10.1016/j.ssnmr.2008.06.003.

[61] I. Chaari, E. Fakhfakh, M. Medhioub, F. Jamoussi, Comparative study on adsorption of cationic and anionic dyes by smectite rich natural clays, J. Mol. Struct. 1179 (2019) 672–677. https://doi.org/10.1016/J.MOLSTRUC.2018.11.039.

[62] D.F. Brito, E.C. da Silva Filho, M.G. Fonseca, M. Jaber, Organophilic bentonites obtained by microwave heating as adsorbents for anionic dyes, J. Environ. Chem. Eng. 6 (2018) 7080–7090. https://doi.org/10.1016/J.JECE.2018.11.006.

[63] F. De Castro Silva, M.M.F. Da Silva, L.C.B. Lima, J.A. Osajima, E.C. Da Silva Filho, Integrating chloroethyl phosphate with biopolymer cellulose and assessing their potential for absorbing brilliant green dye, J. Environ. Chem. Eng. 4 (2016). https://doi.org/10.1016/j.jece.2016.07.010.

[64] S. Gamoudi, E. Srasra, Adsorption of organic dyes by HDPy+-modified clay: Effect of molecular structure on the adsorption, J. Mol. Struct. 1193 (2019) 522–531. https://doi.org/10.1016/J.MOLSTRUC.2019.05.055.

[65] N. Belhouchat, H. Zaghouane-Boudiaf, C. Viseras, Removal of anionic and cationic dyes from aqueous solution with activated organo-bentonite/sodium alginate encapsulated beads, Appl. Clay Sci. 135 (2017) 9–15. https://doi.org/10.1016/J.CLAY.2016.08.031.

[66] C. Tan, G.B. Celli, M.J. Selig, A. Abbaspourrad, Catechin modulates the copigmentation and encapsulation of anthocyanins in polyelectrolyte complexes (PECs) for natural colorant stabilization, Food Chem. 264 (2018) 342–349. https://doi.org/10.1016/J.FOODCHEM.2018.05.018.